

# Imprint of massive neutrinos on Persistent Homology of large-scale structure

M. H. Jalali Kanafi,<sup>1</sup> S. Ansarifard,<sup>2</sup> and S.M.S. Movahed<sup>1,3,\*</sup>

<sup>1</sup>*Department of Physics, Shahid Beheshti University, 1983969411, Tehran, Iran*

<sup>2</sup>*School of Physics, Institute for Research in Fundamental Sciences (IPM), P. O. Box 19395-5531, Tehran, Iran*

<sup>3</sup>*School of Astronomy, Institute for Researches in Fundamental Sciences (IPM), P.O.Box 19395-5531, Tehran, Iran*

(Dated: November 23, 2023)

Exploiting the Persistent Homology technique and an associated complementary representation which enables us to construct a synergistic pipeline for different topological features quantified by Betti curves in reducing the degeneracy between cosmological parameters, we investigate the footprint of summed massive neutrinos ( $M_\nu$ ) in different density fields simulated by the publicly available Quijote suite. Evolution of topological features in the context of super-level filtration on three-dimensional density fields, reveals remarkable indicators for constraining the  $M_\nu$  and  $\sigma_8$ . The abundance of 2-holes is more sensitive to the presence of  $M_\nu$ , also the persistence of topological features plays a crucial role in cosmological inference and reducing the degeneracy associated with  $M_\nu$  simulation rather than their birth thresholds when either the total matter density ( $m$ ) field or those part including only cold dark matter+baryons ( $cb$ ) is utilized. Incorporating the Betti-1 and Betti-2 for  $cb$  part of  $M_\nu^+$  simulation marginalized over the thresholds implies 5% variation compared to the massless neutrinos simulation. The constraint on  $M_\nu$  from  $\beta_k$  and its joint analysis with birth threshold and persistency of topological features for total mass density field smoothed by  $R = 5 \text{ Mpc h}^{-1}$  at zero redshift reach to 0.0172 eV and 0.0152 eV, at  $1\sigma$  confidence interval, respectively.

PACS numbers:

## I. INTRODUCTION

Despite the success of the standard cosmological model,  $\Lambda$ CDM (Among many for example see [1–4]), it is necessary to well constrain the associated extensions in high-precision experiments [5–8]. One of the important extensions to the standard model is called  $\nu\Lambda$ CDM cosmology that is considering the sum of neutrino masses as a free parameter beyond the minimal value [9–11]. From the particle physics point of view, determining the mass of neutrinos is highly motivated [12]. The mass square differences are determined well in three-flavor oscillations analysis of experiments such as reactor, atmospheric, and solar [13]<sup>1</sup>. Though, the absolute mass scale of neutrinos is still unknown. The lower bound on the sum of neutrino mass from oscillation experiments is  $\sum_\nu m_\nu \geq 0.06 \text{ eV}$  for normal and  $\sum_\nu m_\nu \geq 0.1 \text{ eV}$  for inverted hierarchy [14]. On the other hand, the neutrino mass is narrowed down to  $\sum_\nu m_\nu \leq 0.8 \text{ eV}$  at %90 CL from direct detection search [14].

In the cosmology sector, massive neutrinos behave like cold dark matter when they become non-relativistic. They contribute to matter clustering on the scale larger than their free streaming length scale and alternatively, suppress the growth of structures on smaller scales [15]. Therefore their absolute mass has an impact on the distribution of the matter density and the growth rate of the structures as well as the background cosmology. The

background information from Cosmic Microwave Background (CMB) jointly with baryon acoustic oscillation (BAO) and CMB lensing only able to put an upper bound on neutrino mass around 0.6 eV at %95 CL [1]. Moreover, several cosmological observations try to constrain the neutrino mass by estimating the shape and amplitude of the matter power spectrum. However, due to the degeneracy between the neutrino mass and other cosmological or nuisance parameters, the results are not distinctive so far. Among them, CMB primary power spectra in combination with BAO and CMB lensing put a tight upper bound on the neutrino mass which is  $\sum_\nu m_\nu \leq 0.12 \text{ eV}$  at %95 CL [1]. However, this result is weakened to higher mass around  $\sim 0.2 \text{ eV}$  depending on how taking into account the effect of CMB lensing on the CMB primary due to the late-time structures [16, 17]. On the other hand, the current estimators which are utilized for late time universe surveys such as cosmic shear and galaxy clustering are not very powerful enough to well constrain the neutrino mass. Their combination with CMB and BAO shows tending to even more values around  $\sim (0.2 - 2) \text{ eV}$  [18, 19].

The intertwining of parameters on the matter power spectrum makes this analysis weak with respect to adding neutrino mass as a free parameter. In this regard, finding new sophisticated estimators that are able to extract information from observing the matter density would be crucial. More importantly, If new statistics are able to probe different scales, it profoundly provides better results for constraining neutrino mass because of the scale dependency of matter density due to the presence of massive neutrino particles. There have been intensive attempts to clarify different aspects of cosmological infer-

\*Electronic address: m.s.movahed@ipm.ir

<sup>1</sup> <http://www.nu-fit.org/>

ences of neutrino physics and as an illustration, one can mention as follows: The impact of massive neutrinos in the large scale structures with various aspects [20–25]; Cosmic voids in the presence of massive neutrinos [26–29]; Constraining the sum of the active neutrino masses [30, 31]; Incorporating geometrical features to examine the massive neutrinos [32, 33]; Decreasing the degeneracy between the cosmological parameters, particularly the massive neutrinos [34, and references therein]

The intersection of algebraic topology and computational geometry opens an opportunity to shed light and afford deep insight into the quantitative assessment of the various cosmological fields. On the other hand, the appearance of tensions and degeneracies between different cosmological parameters motivated the researchers to consider much more complicated algorithms enabling the systematic evaluation of higher dimensional data. The implementation of some topological invariants such as Euler characteristics and Minkowski Functionals and even their extension which is known as Minkowski Valuations possess more extended experience in cosmological implications [35–40]. Nevertheless, the building blocks of assigning the shape to the discrete and continuous higher-dimensional data through the tilation by the simplicial complexes and computing the various dimensional holes constructed for a given proximity parameter (threshold) have more recently gained considerable attention due to containing strictly more information rather than former measures [41–46](and references therein). The Persistent Homology (PH) in the context of Topological Data Analysis [47–50] which is also known as a shape-based method provides a novel approach associated with the topological invariants to extract information from complex data sets through distinct aspects of underlying structures [51–54]. The PH is a mathematical tool that can be used to analyze and understand the large-scale structure by detecting and tracking the persistency of topological features, such as clusters, filament loops, and voids, across different scales [42, 45, 55–57]. Discriminating between hot and cold dark matter models in the context of persistent homology has been studied by [58]. The non-Gaussianity from a different perspective than other conventional statistical methods using PH has been also carried out by [46, 57, 59]. Besides using the topological measures, some interesting geometrical criteria have been also used for cosmological analysis, particularly to put pristine constraints on the cosmological parameters including the summed massive neutrino [60].

In this work, we are going to explore the subtle effect of massive neutrinos on the large-scale structure (LSS) using some vectorizations of PH. We also carry out the algebra-topological-based approach [61, 62] to constrain  $M_\nu$  and other cosmological parameters. The novelties and advantages of current research are listed below:

(1) We will give a comprehensive constraining on the cosmological parameters including  $M_\nu$  via PH vectorization for total matter density field ( $m$ ) as well as only

cold dark matter and baryons ( $cb$ ) for massive neutrinos simulations.

(2) We also evaluate and finally advocate the potential of PH probe on the reducing degeneracies between various combinations of cosmological parameters, specifically the degeneracy in the plane of  $(M_\nu, \sigma_8)$ .

(3) We also make an efficient estimator inspired by the moment of a typical field and accordingly, we give a quantitative evaluation of the sensitivity of different topological invariants with their cosmological interpretations of neutrino mass.

The rest of this paper is organized as follows. Section II is assigned to review the idea of homology in the context of the excursion set in order to apply it to discrete cosmological data sets. In section III, we present the description of the simulations. Section IV is devoted to probing the signature of massive neutrinos on simulated LSS by Quijote suite. In section V, we quantify the information content of PH to constrain the  $\nu\Lambda$ CDM parameters and total neutrino mass using Fisher analysis formalism. We will give our conclusion in section VI.

## II. PERSISTENT HOMOLOGY

In this section, we describe relevant aspects of Persistent Homology as a tool for quantitative characterization of the morphology of discrete data sets. Suppose that we have a cosmological data set sampled on a cubical lattice,  $\mathcal{M}$ . This data set can consist of the locations of dark matter particles (or dark matter halos) extracted from an N-body simulation or the locations of galaxies obtained from a cosmic survey. For the purposes of this work, we will be dealing with the position of dark matter particles. Let lattice  $\mathcal{M}$  includes  $N_{grid}^3$  regular cubic cells. Having the position of the dark matter particles, we can assign a number density contrast to each cell of the lattice as follows:

$$\delta(\mathbf{r}, t) \equiv \frac{n(\mathbf{r}, t) - \bar{n}(t)}{\bar{n}(t)} \quad (1)$$

where  $n(\mathbf{r}, t)$  represents the number of particles placed in the cell associated to location  $\mathbf{r}$  at cosmic epoch,  $t$ , and  $\bar{n}(t)$  shows the mean number of particles over all cells at  $t$ . It turns out that  $\delta \in [-1, +\infty)$ . Throughout this paper, we fix  $t$  to the present epoch, namely the redshift equates to zero, therefore, we drop the time-dependency of our introduced parameters. Since we are looking for a remarkable gadget to recognize massive neutrinos, therefore redshift dependency evaluation is out of the scope of the current research.

Mathematically, the lattice  $\mathcal{M}$  can be considered as a topological space or more precisely a cubical complex, and  $\delta$  can be interpreted as a map from topological space to real space, indicated by  $\delta : \mathcal{M} \rightarrow \mathbb{R}$ , which  $\mathcal{M} \subset \mathbb{R}^3$ . Applying the definition of the excursion set on  $\mathcal{M}$  in

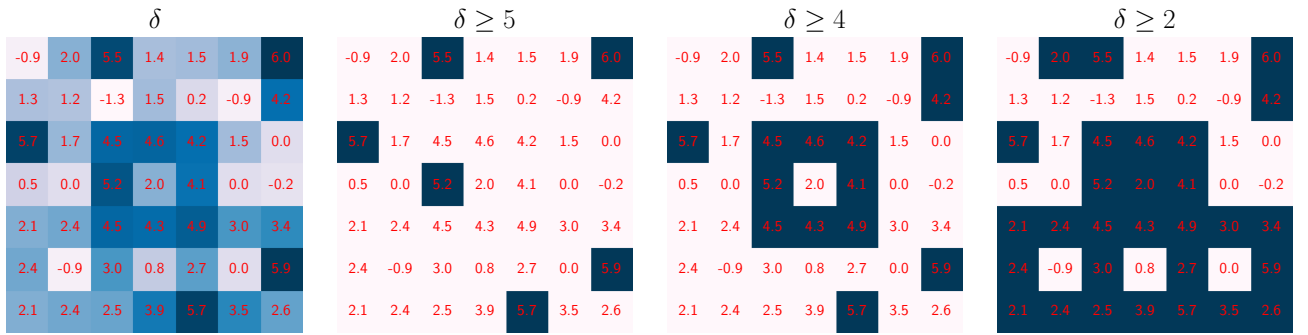


FIG. 1: Evolution of topological features by changing the filtration parameter (known as proximity parameter) in the context of super-level filtration for a 2-dimensional mock density field. The left panel shows the density field and the number assigned to each cell indicates the value of density contrast. The sub-complexes corresponding to the proximity level  $\vartheta = 5, 4, 2$  are indicated in the second, third, and fourth panels from the left, respectively.

the context of super-level filtration leads to the subset  $\mathcal{M}_\vartheta = \{\mathbf{r} \in \mathcal{M} \mid \delta(\mathbf{r}) \geq \vartheta\}$  associated with threshold  $\vartheta$ . Notice that in this work, we have utilized the super-level filtration to perform subsets, however, in a general case, depending on the type of data set, the appropriate filtration should be adopted. By varying the threshold from a minimum value to a maximum value,  $\vartheta_{min} \leq \dots \leq \vartheta_i \leq \vartheta_{i+1} \leq \dots \leq \vartheta_{max}$ , one can obtain a sequence of subsets of  $\mathcal{M}$  as:

$$\mathcal{M}_{\vartheta_{max}} \subseteq \dots \mathcal{M}_{\vartheta_{i+1}} \subseteq \mathcal{M}_{\vartheta_i} \subseteq \dots \mathcal{M}_{\vartheta_{min}} \quad (2)$$

If  $\mathbb{M} = \{\mathcal{M}_{\vartheta_i}\}_i$  denotes the set of subspaces, the main purpose of Topological Data Analysis (TDA), or more specifically Persistent Homology (PH), can be expressed as extracting topological information (topological invariants) from  $\mathbb{M}$ . In algebraic topology, the topological invariant is the term used to describe the global property of a topological space that does not change under the continuous deformation of topological space such as stretching, shrinking, reflecting, rotating, etc. Practically, for our typical topological space ( $\mathcal{M}_{\vartheta_i}$ ) in the context of classical topology, the homology of  $\mathcal{M}_{\vartheta_i}$  characterizes its topological properties. For instance, if  $\mathcal{M}_{\vartheta_i}$  be a 3-dimensional embedded cubical complex, there are 3 homology groups for this space:  $H_k(\mathcal{M}_{\vartheta_i})$  with  $k = 0, 1, 2$ . The Betti numbers,  $\beta_k$ , which are topological invariants, can be determined by the ranks of homology groups:  $\beta_k(\mathcal{M}_{\vartheta_i}) = |H_k(\mathcal{M}_{\vartheta_i})|$ . The elements of the  $k$ th homology group correspond to the  $k$ -dimensional holes ( $k$ -holes) of the cubical complex. The 0-holes, 1-holes, and 2-holes are also known as connected components, loops, and voids, respectively. Therefore, the Betti numbers give the number of connected components, loops, and voids of a topological space. In the classical topology, filtration does not play a role, but TDA and PH as its main ingredients, considering the concept of filtration, are designed to generalize the notion of the classical topology and accordingly apply it to discrete data sets.

As mentioned earlier, the filtration procedure constructs a set of (sub-)cubical complexes ( $\mathbb{M}$ ) to the dis-

crete data set. A trivial way to study  $\mathbb{M}$  set is extracting the topological properties of its sub-complexes through their homology groups ( $H_k(\mathcal{M}_{\vartheta_i})$ ), separately. Although, PH provides an approach which in addition to the capture of information of each sequence, quantifies the evolution of topological features by changing the filtration parameter and subsequently inclusion maps  $\mathcal{M}_{\vartheta_i} \rightarrow \mathcal{M}_{\vartheta_{i+1}}$ . By the term evolution, we mean the appearance (*birth*) and disappearance (*death*) of topological features by changing the filtration parameter. The persistent homology of  $\mathbb{M}$  is given by  $H_k(\mathbb{M})$ , which contains information in the form of persistent pair  $\vartheta^{(k)} = (\vartheta_{birth}^{(k)}, \vartheta_{death}^{(k)})$ . A persistent pair indicates that a  $k$ -hole is born at level  $\vartheta_{birth}^{(k)}$  and dies at level  $\vartheta_{death}^{(k)}$ . The information of persistent homology can be summarized in a multiset as  $\mathcal{D}_k = \left\{ \vartheta_i^{(k)} \right\}_i$  which is a collection of all persistence pairs and is known as persistence diagram. In Fig. 1, we illustrate the density contrast field of a 2-dimensional toy data set. The field are sampled between  $-1 \leq \delta \leq 6$  and some its sub complexes obtained from performing filtration are visualized as well. By reducing the value of proximity parameter the  $k$ -holes are appeared and also at some other thresholds they merge together and therefore they are disappeared. We can also define:

$$\vartheta_{(i),pers}^{(k)} \equiv \left| \vartheta_{(i),death}^{(k)} - \vartheta_{(i),birth}^{(k)} \right| \quad (3)$$

to measure the persistency of a pair. Therefore the combination of two of the three  $\vartheta_{(i),birth}^{(k)}$ ,  $\vartheta_{(i),death}^{(k)}$  and,  $\vartheta_{(i),pers}^{(k)}$  as a persistence diagram provide topological information of the underlying field. Although multiset  $\mathcal{D}_k$  contains the persistent homology information and can be used for demonstration purposes, in order to achieve quantitative results for further analysis, we need to use statistical criteria defined over the persistence pairs. There are some criteria that have been introduced for statistical analysis of the PH [54]. In the rest of this

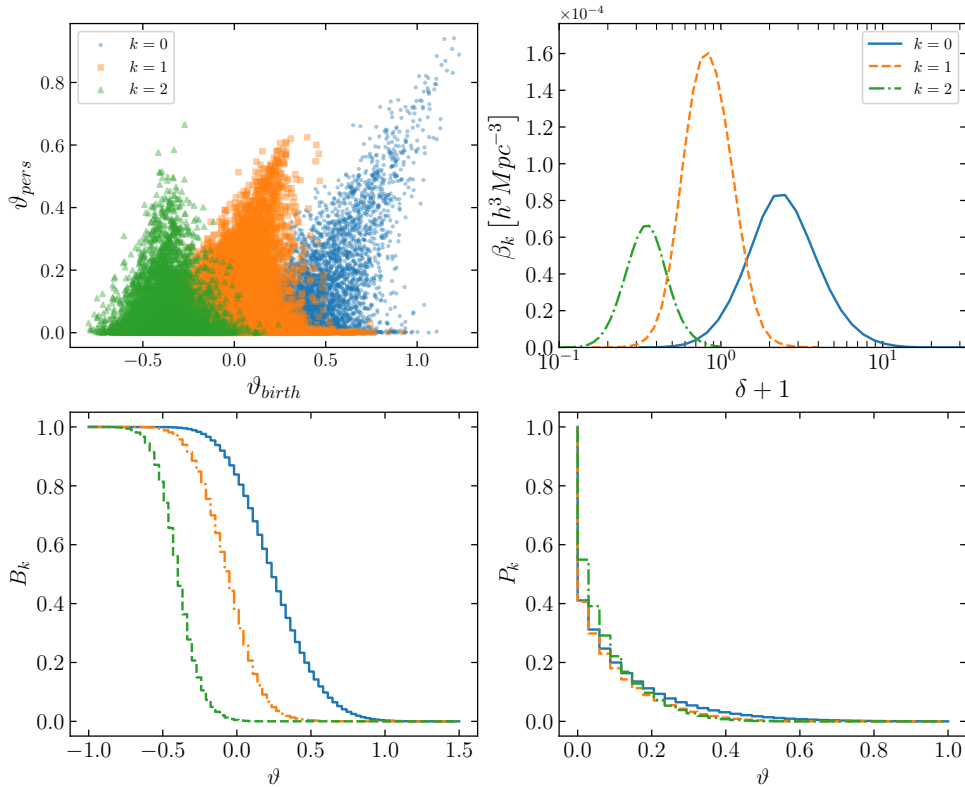


FIG. 2: This plot shows the extracted persistence diagram of a fiducial realization from Quijote simulations.

section, we attempt to have a brief review of some of such criteria. We begin with the well-known Betti curves, accordingly, they can be considered as the collections of all Betti numbers which are extracted from sequences (sub-complexes) and sorted by filtration parameter. In fact, Betti curves visualize the evolution of the  $k$ -holes' populations through the  $\vartheta$ . In the context of persistence pairs, for a fixed  $\vartheta$ , the  $\beta_k(\vartheta)$  can be given as the number of pairs which satisfy conditions  $\vartheta_{(i),birth}^{(k)} \geq \vartheta$  and  $\vartheta_{(i),death}^{(k)} \leq \vartheta$ . Mathematically, this can be written as

$$\beta_k(\vartheta) = \sum_{i=1}^{n_k} \Theta\left(\vartheta_{(i),birth}^{(k)} - \vartheta\right) \Theta\left(\vartheta - \vartheta_{(i),death}^{(k)}\right) \quad (4)$$

where  $\Theta(\cdot)$  indicates Heaviside function, and  $n_k$  represents the total number of persistence pairs related to the  $k$ th persistence diagram. Throughout this paper, we divide the  $\beta_k$  by the box size, and hereafter, we call them the normalized Betti numbers. It is worth noting that Betti curves do not contain all the information encoded in the persistence diagrams. Therefore in order to provide complementary information, we are going to use two classes of such visualizations which were first proposed by [57].

These visualizations, which are denoted by  $B_k(\vartheta)$  and  $P_k(\vartheta)$ , can be given by the number of persistence pairs passing specific conditions,  $\vartheta_{(i),birth}^{(k)} \geq \vartheta$  and  $\vartheta_{(i),pers}^{(k)} \geq \vartheta$

for  $B_k(\vartheta)$  and  $P_k(\vartheta)$ , respectively. The mathematical descriptions of  $B_k(\vartheta)$  and  $P_k(\vartheta)$  become:

$$B_k(\vartheta) \equiv \sum_{i=1}^{n_k} \Theta\left(\vartheta_{(i),birth}^{(k)} - \vartheta\right) \quad (5)$$

and

$$P_k(\vartheta) \equiv \sum_{i=1}^{n_k} \Theta\left(\vartheta_{(i),pers}^{(k)} - \vartheta\right) \quad (6)$$

To report the  $B_k$  and  $P_k$  for underlying data sets, we use the empirical distribution function as the numerical estimator for the mentioned topological measures. In the next section, we will rely on the quantitative measures of topological properties, and therefore based on a pipeline, we will implement the PH vectorization on the mock data for cosmological inferences.

### III. DATA DESCRIPTION

In this work to prob the imprints of massive neutrinos on the LSS using the PH, we use a subset of simulations from the Quijote suite [63]. The Quijote simulations consist of 44100 N-body realizations. The Tree+SPH code GADGET-III is used to generate all realizations of the

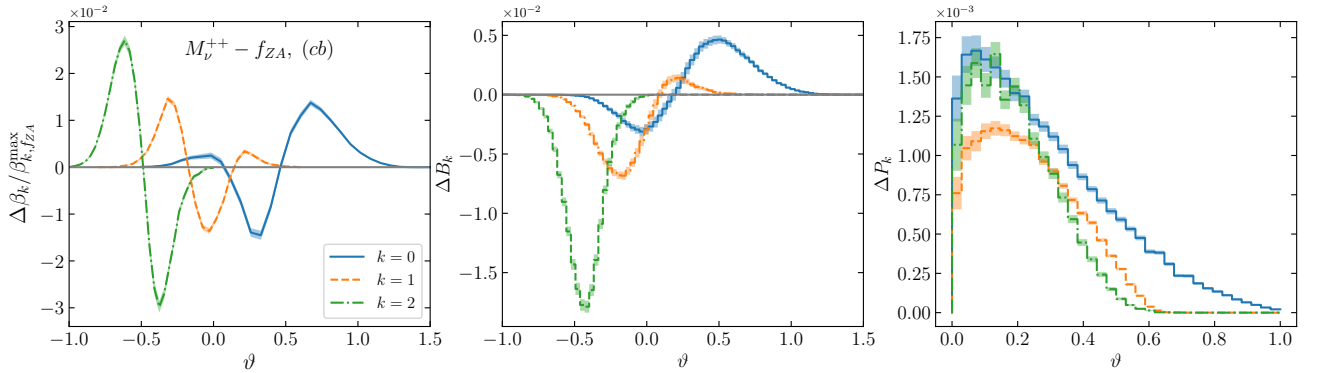


FIG. 3: The PH vectorization is derived from the  $cb$  field when the massive neutrinos particles with the total mass  $M_\nu^{++} = 0.2$  eV are added compared to the fiducial cosmology. The upper panel represents the Betti curves divided by the corresponding maximum value in the fiducial case. The middle and lower panels are devoted to the differences in the  $(B_k, P_k)$ , respectively. The blue solid, orange dashed and green dashed-dotted lines represent the 0-hole, 1-hole, and 2-hole homology groups respectively. The shaded areas are corresponding to the  $2\sigma$  confidence interval errors.

Quijote simulations. All simulations consist of  $512^3$  gravitationally interacting dark matters (for simulations with massive neutrinos there are also  $512^3$  neutrino particles) which are sampled on the cubical volume of  $1 \text{ Gpc}^3 h^{-3}$  with periodic boundary condition. The redshift interval for the simulation is  $z \in [0, 127]$ . To generate the initial conditions of simulation with massive neutrinos (also for their fiducial massless counterparts) the rescaling method [64] and Zeldovich's approximation are used, however for all other simulations, second-order perturbation theory is employed. The cosmological parameters related to the fiducial simulations are based on the flat  $\Lambda$ CDM including  $\Omega_m = 0.3175$ ,  $\Omega_b = 0.049$ ,  $h = 0.6711$ ,  $n_s = 0.9624$  and  $\sigma_8 = 0.834$  in a good agreement with [1].

To examine the various aspects of massive neutrinos, one can focus on the total matter field including cold dark matter (CDM), baryons, and neutrinos. In addition, due to the influence of massive neutrinos on the evolution of CDM and baryons field, it is possible to rely on the CDM+baryons in the simulation providing a studied field. Hereafter, we denote the former field with  $m$  and the latter one with  $cb$ , which are familiar in this context. We will see soon in the next section, the motivation for choosing the mentioned fields for cosmological applications. The total mass of neutrino particles in the Quijote simulations for massive neutrinos is categorized into  $M_\nu^+ = 0.1$  eV,  $M_\nu^{++} = 0.2$  eV and  $M_\nu^{+++} = 0.3$  eV.

We also utilize the `Pylians` [65] routines to construct density contrast fields from Quijote snapshots for both  $m$  and  $cb$  fields. We adopt a cloud-in-cell (CIC) mass-assignment scheme to construct fields on regular grid spacing. Also, we smooth density contrast fields using a Gaussian smoothing kernel with smoothing scale  $R = 5 \text{ Mpc } h^{-1}$  to reduce shot noises.

#### IV. IMPLEMENTATION OF PH ON THE QUIJOTE N-BODY SIMULATIONS

In this section, we present the topological information including  $(\beta_k, B_k, P_k)$  computed for a subset of Quijote simulations for different cosmological models.

##### A. PH of fiducial cosmology

Before addressing the effect of changing the desired cosmological parameters on the topological criteria, for the sake of clarity, we depict the persistence diagram and associated vectorization corresponding to a realization of the fiducial simulations in Fig 2. The upper left panel illustrates the persistence diagram in the scatter plot style in the birth-persist coordinate. Each of the blue circles, orange squares and green triangles represents a persistence pair  $(\vartheta_{(i),birth}^{(k)}, \vartheta_{(i),pers}^{(k)})$  corresponding to the 0-, 1- and 2-holes, respectively. It can be realized that 0-holes mainly appear at higher thresholds than 1-holes and even 2-holes. Also the 0-, 1- and 2-holes mainly appear at the high, the middle, and the low thresholds, respectively. Mentioned behavior can be justified based on the nature of connected components (clusters), filaments, and voids which are topologically quantified by  $\beta_0$ ,  $\beta_1$ , and  $\beta_2$ , respectively. Also, this panel indicates that the connected components have more persistency rather than filaments and voids. In other words, the tendency of the persistence diagram for 0-hole is due to the fact that the higher value of  $\vartheta_{birth}$  possesses the higher value of  $\vartheta_{pers}$  leading to the higher density regions to be more persistent against the filtration process in analogous the temporal evolution of hierarchical clustering. In the upper right panel of Fig 2, we plot the extracted  $\beta_k$  from the fiducial realization as a function of filtration

density  $\delta + 1 = 10^\vartheta$  for better visualization<sup>2</sup>. The blue solid line, orange dashed line and green dashed-dotted line indicate the  $\beta_0$ ,  $\beta_1$ , and  $\beta_2$ , respectively. The number of independent topological features gradually grows as the filtration threshold is reduced until they eventually achieve their own maximum value. Finally, as the proximity parameter decreases towards the field's minimum value, the number of topological components decreases. The lower panels of Fig 2 show the  $B_k$  and  $P_k$  versus threshold, confirming the representative behavior of the persistence diagram (upper left panel), quantitatively.

## B. Imprint of Massive neutrinos on PH

In the previous subsection, we dealt with the topological properties of the fiducial model in Quijote simulations and we realized the overall behavior of  $(\beta_k, B_k, P_k)$ . Now, we will turn to examine the influence of massive neutrinos on simulated density fields through our PH vectorization. Before going further, we take a look at what we would expect by the impact of summed massive neutrinos in the topological invariants of the density field when the sub-level filtration is performed. Having the large thermal velocities of massive neutrinos on one hand, and on the other hand, the reducing the conventional dark matter density in the total mass content of the universe, conduce the massive neutrino particles are less clustered, particularly on scales below their so-called free-streaming scale. This also would be supported due to the decreasing depth of total matter potential wells in the vicinity of massive neutrinos. As a result, we would expect the signature of massive neutrinos to appear in all topological invariants in different manners for  $m$  and  $cb$  fields. The presence of massive neutrino particles directly changes the  $m$  field which is a relevant observable made by the surveys that observe the total matter field through the weak lensing effect [66]. The analysis of  $cb$  field is also motivated by products of those surveys measuring the clustering of halos or galaxies [4]. In this subsection, the statistics defined in the previous section namely  $(\beta_k, B_k, P_k)$  are applied to both  $m$  and  $cb$  fields in the presence of massive neutrino particles and compared to the fiducial in order to quantify the footprint of neutrino mass on the associated simulated fields.

At first, we compute the  $\beta_k$ ,  $B_k$ , and  $P_k$  measures over the  $cb$  field when the massive neutrino particles are included in the fiducial simulation. The differences with respect to the fiducial are shown in Fig 3. Here we consider the case  $M_\nu^{++} = 0.2$  eV for the neutrino cosmology. The left panel of Fig 3 illustrates the Betti-curves versus threshold. For better visualization, we divide the  $\beta_k$  by  $\beta_{k, f_{ZA}}^{\max}$ , where the subscript “ $f_{ZA}$ ” means the Zel’dovich

approximation fiducial model [63]. The maximum difference occurs for the  $\beta_2$  (2-hole) that is shown as a green dashed-dotted line in the left panel of Fig 3. It suggests that the topological properties of voids are proper tracers to probe the effect of neutrino mass in the LSS which is consistent with the interplaying of massive neutrinos. From other quantitative points of view, we also plot the  $B_k$  and  $P_k$  in the middle and right panels of Fig. 3, respectively. It is worth noting that the effect of neutrino mass varies from 0.1% to 3% for the PH vectorization in the range of density contrast thresholds for  $M_\nu^{++} = 0.2$  eV. To interpret our results, we should first notice the properties of the Quijote simulations. A key note is that including the massive neutrino particles in the corresponding pipeline for the Quijote suite is supposed to satisfy the fixed value for the  $\sigma_8$  condition compared to the fiducial simulations. In addition, based on the adopted approach for simulation, the change in the  $\sigma_8$  is carried out by tuning the  $A_s$ . Therefore, the  $\sigma_8$  of  $cb$  (CDM+baryons) field, which is denoted by  $\sigma_8^{(cb)} = 0.846$ , is greater than the fiducial value, namely  $\sigma_8 = 0.834$  for the Quijote massive neutrinos simulations. Subsequently, the presence of massive neutrino particles in the density field does not only vary the population of the  $k$ -hole, but also, changes the persistence pairs from topological properties points of view. It means that more number of birth is expected at higher thresholds for the 0-holes, while the 2-holes mostly appear in the lower thresholds. We also expect to have a migration in the population of 2-holes from higher mass thresholds to the lower mass represented by  $\beta_2$  curve, whereas, this situation behaves in the opposite way for the connected component quantified by  $\beta_0$  plot (the blue solid line) and the peak location of the 0-hole population moves toward the higher mass regions. The enhancement on both tails and a reduction in the averaged threshold are seen for the case of  $\beta_1$  curve that corresponds to the filaments (the orange dashed line).

According to the functional form of the  $\sigma_8$ , it is well-known that this quantity would possibly mimic the effect of massive neutrino particles leading to degeneracy in the plane of  $(M_\nu, \sigma_8)$  at least when considering the standard two-point clustering statistics [67, 68]. Therefore, it is important to check how the PH vectorization responds to such degeneracy. To address this issue, we use another subset of the Quijote simulation dubbed by  $\sigma_8^+ = 0.849$  without the massive neutrinos. It turns out that the  $\sigma_8^+$  of this specific subset is close to the  $\sigma_8^{(cb)}$  that is for  $cb$  field of the  $M_\nu^{++}$  simulation. Now, we turn to compare the behavior of PH vectorization for available fields including the massive neutrinos, namely  $m$  and  $cb$  with that case for which the  $M_\nu = 0$  with  $\sigma_8^+$ . In other words, we look for any promising signature via PH lens for breaking or at least reducing the degeneracy between  $\sigma_8$  and  $M_\nu$ . Fig. 4 indicates the  $\beta_k$  (upper panels),  $B_k$  (middle panels) and  $P_k$  (lower panels) versus  $\vartheta$ . The blue solid line corresponds to the difference between results for the

<sup>2</sup> Throughout the analysis of Quijote field we first map the  $\delta$  to the  $\log(\delta + 1)$  and then apply the filtration.

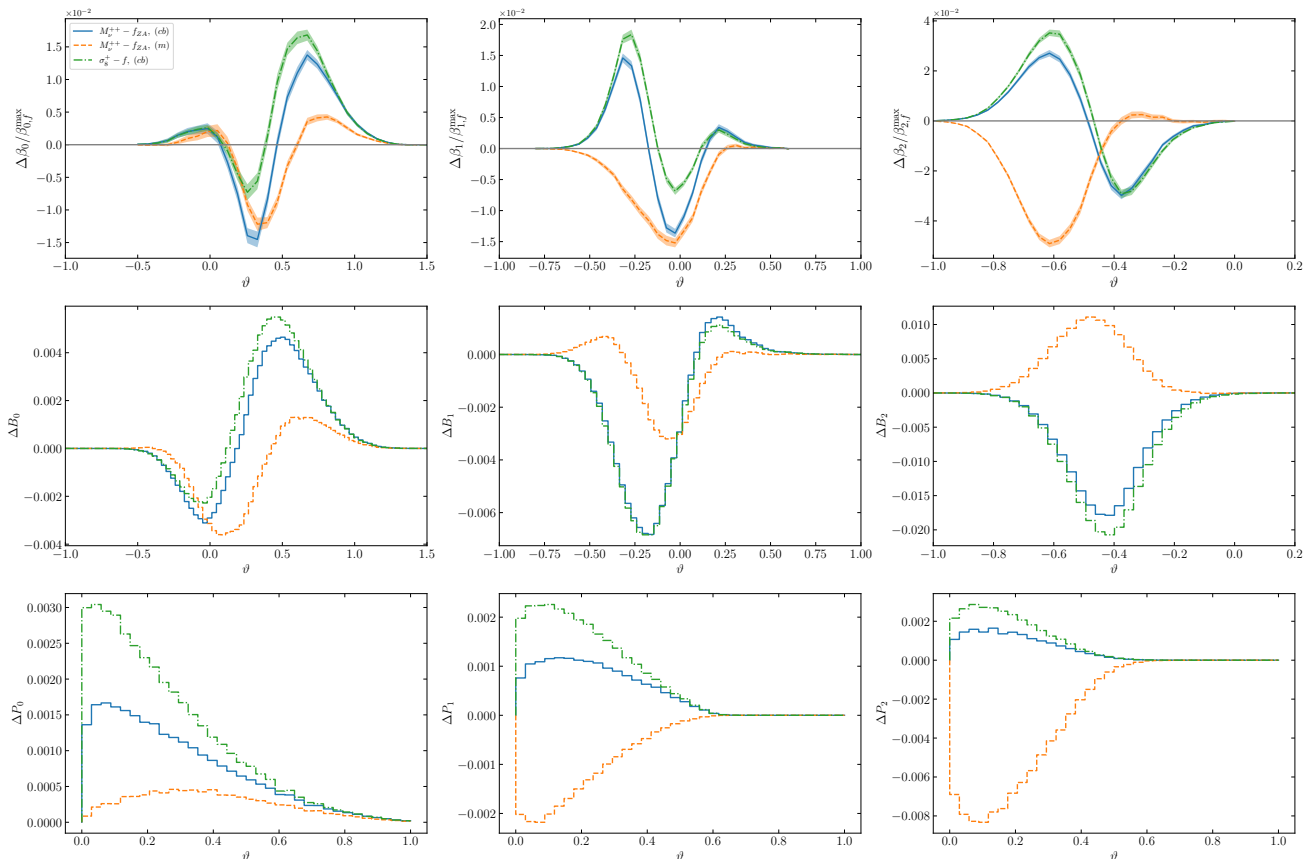


FIG. 4: Impact of massive neutrinos on the various quantitative measures in the banner of PH. The upper panels indicate results for betti curves, while the middle panels are for  $B_k$ . The lower panels illustrate the  $P_k$ . The blue solid line corresponds to the difference between  $cb$  part of  $M_\nu^{++}$  simulation and fiducial cosmology. The orange dashed line is similar to the blue solid curve just for the total matter density field. The green dashed-dotted is associated with  $\sigma_8^+$  simulation.

PH measures applied on the  $cb$  part of the field including the massive neutrinos ( $M_\nu^{++}$ ) and fiducial model, while the orange dashed line is associated with  $m$  field. The green dashed-dotted line shows for field with  $\sigma_8^+$  in the absence of the massive neutrinos. The overall behavior of  $(\beta_k, B_k, P_k)$  for  $cb$  field for both  $\sigma_8^+$  and  $M_\nu^{++}$  simulations are almost similar, however, from a quantitative point of view, the  $P_k$  reveals almost 50% relative difference. The 1- and 2-holes statistics for  $m$  field demonstrate distinguished behavior compared to  $cb$  and  $\sigma_8^+$  simulations. Combining the non-linearity as well as suppression process due to the contribution of massive neutrino on the matter density field convinces the existence of different trends of  $\beta_k$  for  $k = 1, 2$  for  $m$  compared to  $cb$  part. Topological behavior encoded by  $\beta_0$  shows population migration from intermediate thresholds to high and low thresholds accompanying the deficiency compared to the fiducial field, while for Betti-2, which mainly has the value for the range of  $-1 \lesssim \vartheta \lesssim 0$ , we almost obtain the deficiency for massive neutrinos simulation respect to the massless neutrinos cosmology. The mentioned behavior will be also demonstrated by the Fisher forecasts analysis in the next section.

In order to achieve a quantitative measure for evaluating the signature of massive neutrinos based on PH vectorization, we integrate out the  $\vartheta$ -dependency through the moment definition as:

$$\Xi_k^{(n)} \equiv \int d\vartheta \vartheta^n \mathcal{P}(\beta_k(\vartheta)) \quad (7)$$

where  $\mathcal{P}$  is the probability density function computed for  $\beta_k$ . Accordingly, we define  $\mathcal{R}_k^{(n)} \equiv (\Xi_{k, M_\nu^+}^{(n)} - \Xi_{k, fid}^{(n)}) / (\Xi_{k, fid}^{(n)})$  and plot this quantity for  $cb$  field of  $M_\nu^+$  simulation in Fig. 5. The signature of massive neutrinos in the 1- and 2-holes are higher than the connected component captured by  $\beta_0$ , as an illustration for  $n = 5$ , we obtain almost  $\sim 5\%$  and  $\sim 2.5\%$  when the  $\beta_{(1,2)}$  and  $\beta_0$  are adopted, respectively.

## V. QUANTIFYING INFORMATION CONTENT: FISHER FORECASTS

In this section, relying on the Fisher matrix analysis, we quantify the capability of topological measures

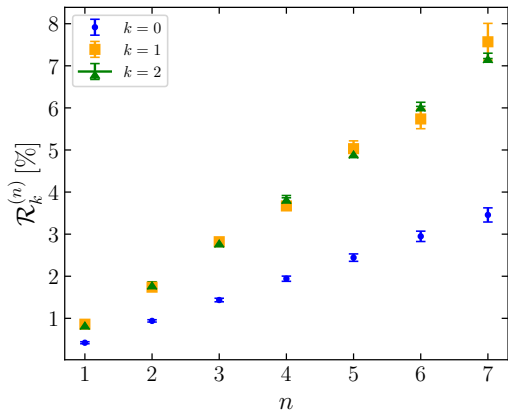


FIG. 5: The percentage relative difference of Betti moments for  $cb$  part of  $M_\nu^+$  simulation with respect to the fiducial field. The blue filled circle, orange filled square, and green filled triangle symbols are for  $\beta_0$ ,  $\beta_1$ , and  $\beta_2$ , respectively.

$(\beta_k, B_k, P_k)$  and their combinations on constraining the cosmological parameter denoted by a row vector as  $\theta$ :  $\{\Omega_m, \Omega_b, \sigma_8, h, n_s, M_\nu\}$ . The element of the Fisher information matrix is defined by:

$$F_{mn} = - \left\langle \frac{\partial^2 \ln \mathcal{L}}{\partial \theta_m \partial \theta_n} \right\rangle \quad (8)$$

where  $\mathcal{L}$  is the Likelihood distribution. Assuming the multivariate normal distribution for the Likelihood function, we have:

$$F_{mn} = \frac{\partial \mathcal{A}^T}{\partial \theta_m} C^{-1} \frac{\partial \mathcal{A}}{\partial \theta_n} \quad (9)$$

where  $\mathcal{A}$ :  $\{\beta_k, B_k, P_k\}$  and any desired combinations of its elements. The  $C$  indicates the covariance matrix, and it is computed over 5000 realizations of the fiducial simulations in our pipeline. To calculate the partial derivative of the vector  $\mathcal{A}$  with respect to the cosmological parameters, we use the following approximation:

$$\frac{\partial \mathcal{A}}{\partial \theta_m} \simeq \frac{\mathcal{A}(\theta_m^+) - \mathcal{A}(\theta_m^-)}{\theta_m^+ - \theta_m^-} \quad (10)$$

where  $\mathcal{A}(\theta_m^+)$  and  $\mathcal{A}(\theta_m^-)$  represent the extracted data vectors from simulations in which the value of their  $\theta_i$  parameter is higher and lower than the fiducial value, respectively. Also, to calculate the partial derivative with respect to  $M_\nu$ , we use:

$$\frac{\partial \mathcal{A}}{\partial M_\nu} \simeq \frac{\mathcal{A}(M_\nu^+) - \mathcal{A}(\theta_{ZA})}{0.1} \quad (11)$$

where  $\mathcal{A}(M_\nu^+)$  indicates the obtained data vector from massive neutrinos stimulation with  $M_\nu = 0.1$  eV, and  $\mathcal{A}(\theta_{ZA})$  represent the extracted data vectors from fiducial simulations which their initial conditions are generated with Zel'dovich approximation. To estimate the

partial derivatives, for each of the model parameters that have a different value from the fiducial value, we have used 500 corresponding realizations (for more details see [63]).

Our analysis will be exploited by considering redshift  $z = 0$  and smoothing scale  $R = 5$  Mpc  $h^{-1}$ . We begin our investigation with constraining on the pair parameters  $M_\nu$  and  $\sigma_8$ . Fig. 6 is devoted to the marginalized 68% and 95% confidence contours for  $M_\nu$  and  $\sigma_8$  parameters for  $cb$  and  $m$  fields. The upper row illustrates the constraints for the  $cb$  density field, while the lower row shows the constraints for the  $m$  density field. In the upper left column, we consider the various components of Betti curves including  $\beta_0$ ,  $\beta_1$ , and  $\beta_2$ , and the associated joint analysis as the observable vector. The middle and right columns are the same as the left column, but for the  $B_k$  and  $P_k$  vectorization, respectively. For the  $cb$  field the directions of degeneracy between  $M_\nu$  and  $\sigma_8$  constraints obtained from various components of PH measures approximately are similar, and this degeneracy also remains for the constraints resulting from their combinations which is in agreement with the results indicated in Fig. 4. However, for the  $m$  density field, the mentioned degeneracy directions are different, which leads to reducing the degeneracy between  $M_\nu$  and  $\sigma_8$  for the compound constraints. In Fig. 7, we compare the obtained constrains from joint analysis,  $\beta + P + B$ , on  $(M_\nu, \sigma_8)$  parameters for  $cb$  and  $m$  density fields. Obviously, it confirms that the constraints are tighter in the  $m$  field compared to the  $cb$  field leading to reducing the degeneracy between  $M_\nu$  and  $\sigma_8$ . To make more complete our analysis, we show the 2D constrains (at 68% and 95% confidence level) on most relevant  $\nu\Lambda$ CDM parameters ( $M_\nu, \sigma_8, \Omega_m, \Omega_b, h, n_s$ ) derived from the Fisher analysis for only  $\beta$  and the joint probes,  $\beta + B + P$ , for  $cb$  field in the left panel of Fig. 8. The same results are depicted in the right panel of Fig. 8 for  $m$  field. Applying the joint analysis  $\beta + P + B$  shows almost two times improvements in constraining the cosmological parameters compared to the  $\beta$  for  $cb$  field. We also summarized the marginalized 68% errors on the cosmological parameters obtained from some different probes in Table I for better comparison, quantitatively. Comparing the power of PH measures to put constraints on the massive neutrinos with e.g. Minkowski Functionals (MFs), reveals that for the  $cb$  field, we achieve considerable improvement, while the computed uncertainty in the  $m$  field remains almost the same as MFs [24].

We performed PH calculations using `Cubical ripser` [69], and `GUDHI` [70] python packages. Also, we utilized `Getdist` python package [71] to provide the Fisher forecast plots.

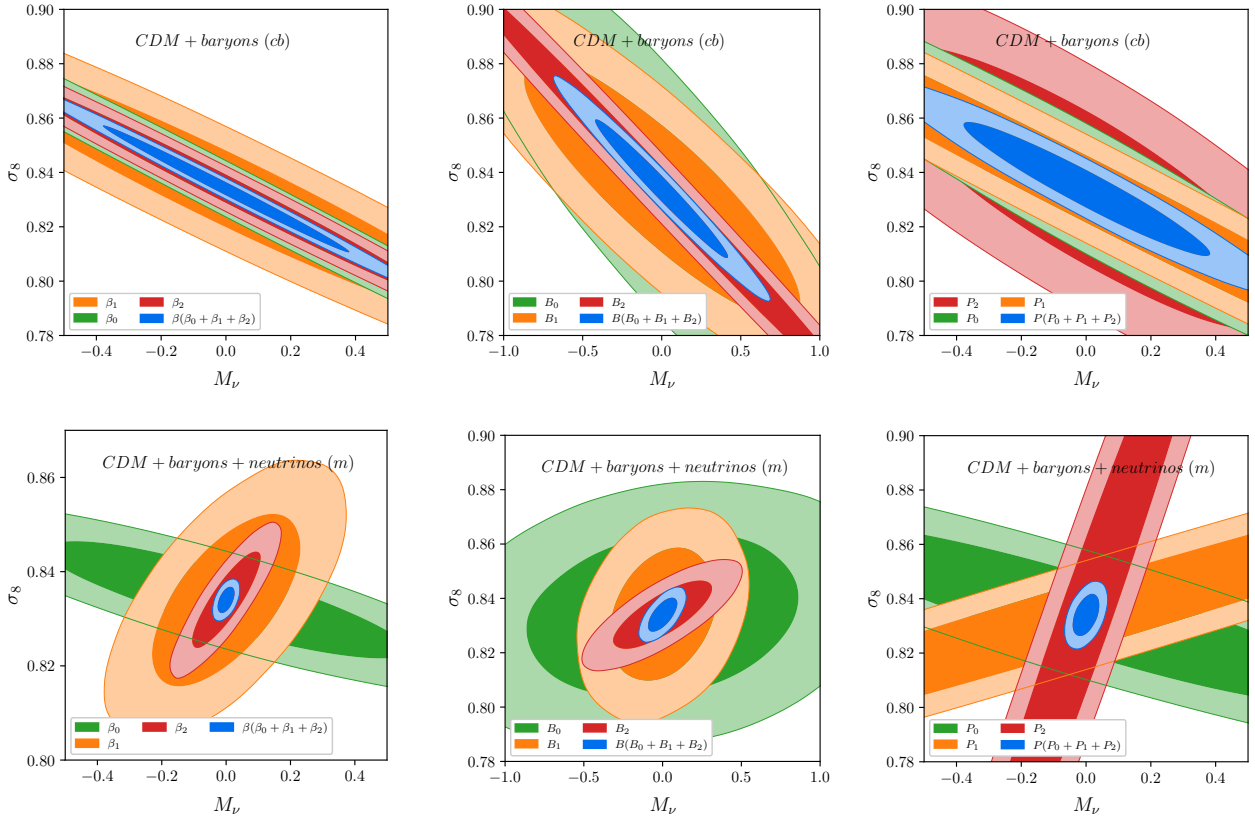


FIG. 6: The 68% and 95% confidence contours for  $(M_\nu, \sigma_8)$  obtained from various measures under the PH for both  $cb$  and  $m$  fields at redshift  $z = 0$  by the Fisher information analysis. The upper row panels depict constraints for  $cb$  field, while the bottom row panels are devoted to showing  $m$  field constraints. Taking into account the total matter density field causing reducing the degeneracy in the plane of  $(M_\nu, \sigma_8)$ , considerably.

Statistics (field)	$M_\nu$ (eV)	$\sigma_8$	$\Omega_m$	$\Omega_b$	$h$	$n_s$
$\beta$ ( $cb$ )	0.2504	0.0153	0.0442	0.0156	0.1546	0.0699
$\beta$ ( $m$ )	0.0172	0.0018	0.0427	0.0152	0.1617	0.0747
$P$ ( $cb$ )	0.2511	0.0162	0.0559	0.0163	0.1640	0.1128
$P$ ( $m$ )	0.0269	0.005	0.0564	0.0163	0.1650	0.1224
$B$ ( $cb$ )	0.2779	0.0168	0.062	0.0163	0.1380	0.1694
$B$ ( $m$ )	0.0610	0.0041	0.0615	0.0139	0.1709	0.1473
$\beta + P + B$ ( $cb$ )	0.1242	0.0077	0.027	0.0075	0.0878	0.0423
$\beta + P + B$ ( $m$ )	0.0152	0.0015	0.0267	0.0075	0.0886	0.0436

TABLE I: The uncertainty interval computed by marginalization in the Fisher forecasts for the cosmological parameters at 68% level of confidence.

## VI. CONCLUSIONS

Motivated by various theoretical approaches and observational pipelines for evaluating the neutrino oscillation and associated masses, in addition to pondering the massive neutrinos has a dominant influence on small scales of structure formation, we have relied on the Betti numbers as a set of topological invariants and a com-

plementary quantitative measures proposed by [57], to deal with N-body simulations of Quijote suite for massive neutrinos cosmology. For different cosmological simulated fields, namely total mass density field ( $m$ ), the CDM+baryons part in the presence of  $M_\nu$ , we have computed  $(\beta_k, B_k, P_k)$ . Comparing this PH vectorization between massive neutrinos simulation and the fiducial case revealed that the voids are more sensitive tracers to probe the footprint of neutrino mass scale in the large-scale

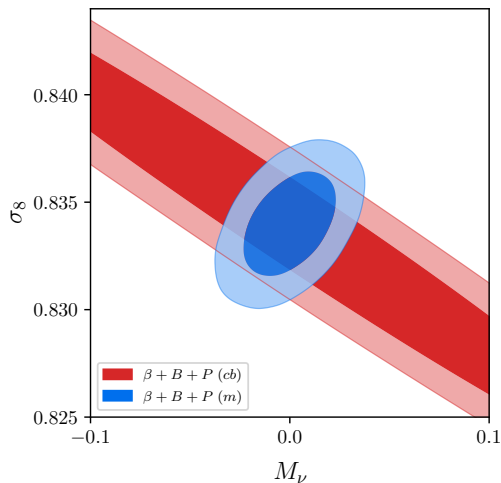


FIG. 7: Fisher forecast based on the joint analysis of  $\beta+B+P$  for  $cb$  and  $m$  fields at  $1\sigma$  and  $2\sigma$  confidence intervals.

structure when the topological measures are used (see Fig. 3). Our results confirmed that the effect of neutrino mass varies the PH vectorization more than 2%. The degeneracy between  $\sigma_8$  and  $M_\nu$  is another challenge when the two-point statistics of LSS is considered to examine the massive neutrinos. Therefore to elucidate whether the PH vectorization introduced in this paper is able to resolve or at least to reduce this discrepancy, we have exploited two simulations  $\sigma_8^+$  and  $M_\nu^{++}$ . According to the results presented in Fig. 4, One can see the same behaviors on PH measures for these two simulations. The promising achievement, however, is that the persistency of topological features is the more reliable criterion to mitigate the influence of the mentioned degeneracy rather than the birth threshold of features (see lower row of Fig. 4). At the non-linear regime, the contribution of massive neutrinos on  $\beta_0$  and  $\beta_2$  demonstrated controversial behavior when the total matter density field was to be considered. Marginalization over the thresholds contribution in Betti-curves also confirmed that the higher rank of Betti numbers are proper candidates for probing the massive neutrinos (Fig. 5).

We followed our analysis by computing the Fisher information matrix to assess the capability of topological measures to constrain the relevant cosmological parameters. Betti curves as one of the PH vectorization compo-

nents have shown better constraining on the parameters with respect to the other measures. The combinations improve the constraints around twice for the  $cb$ . However, using the  $cb$  field, the degeneracy in the plane of  $(M_\nu, \sigma_8)$  remains. Adding new information for example by studying more than one map which brings the direct evolutionary footprint of the field is suggested in this case. There is no similar degeneracy seen for the case of the  $m$  field (Figs. 6, 7, 8 and Table I).

Finally, our study demonstrates the potential of persistent homology as a valuable tool for analyzing complex cosmological datasets and extracting information about the impact of massive neutrinos on large-scale structure. This approach shows the power to constrain well the neutrino mass along with the other cosmological parameters. Therefore, it is able to complement previous methods and offers a fresh perspective on understanding the mass hierarchy of the active neutrinos. Thanks to the high capability of the PH approach to reveal the impact of a variety of scales in a field, it is worth considering the application of this method to the current and upcoming high-precision cosmological surveys in order to study different scenarios even beyond the active three flavor scheme. To do more complementary analysis, we can list the following suggestions: in this paper, we have fixed the smoothing scale and it is useful to incorporate various values of scale and check the robustness of PH vectorization. The redshift dependency is also another interesting part to do for another study. Quantifying the information, content usually is carried out by Fisher forecasts, while an alternative approach so-called simulation-based inference (SBI) known as a likelihood-free analysis also is useful to implement [72–74]. Combining the PH measures with other observable quantities enables us to confine the uncertainty of cosmological parameters which is another motivated topic for high-precision evaluations.

### Acknowledgments

SMSM and SA appreciate the hospitality of the HECAP section of ICTP where part of this research was completed. We also thank the Quijote team for sharing its simulated data sets and providing extensive instruction on how to utilize the data.

- 
- [1] N. Aghanim, Y. Akrami, M. Ashdown, J. Aumont, C. Baccigalupi, M. Ballardini, A. Banday, R. Barreiro, N. Bartolo, S. Basak, *et al.*, *Astronomy & Astrophysics* **641**, A6 (2020).
  - [2] S. Alam *et al.* (eBOSS), *Phys. Rev. D* **103**, 083533 (2021), arXiv:2007.08991 .
  - [3] D. Brout *et al.*, *Astrophys. J.* **938**, 110 (2022), arXiv:2202.04077 .
  - [4] D. E. Survey, K.-D. S. Collaboration, T. Abbott, M. Aguena, A. Alarcon, O. Alves, A. Amon, F. Andrade-Oliveira, M. Asgari, S. Avila, *et al.*, arXiv preprint arXiv:2305.17173 (2023).
  - [5] R. Laureijs, J. Amiaux, S. Arduini, J.-L. Augeres, J. Brinchmann, R. Cole, M. Cropper, C. Dabin, L. Duvet, A. Ealet, *et al.*, arXiv preprint arXiv:1110.3193 (2011).
  - [6] P. A. Abell, J. Allison, S. F. Anderson, J. R. Andrew,

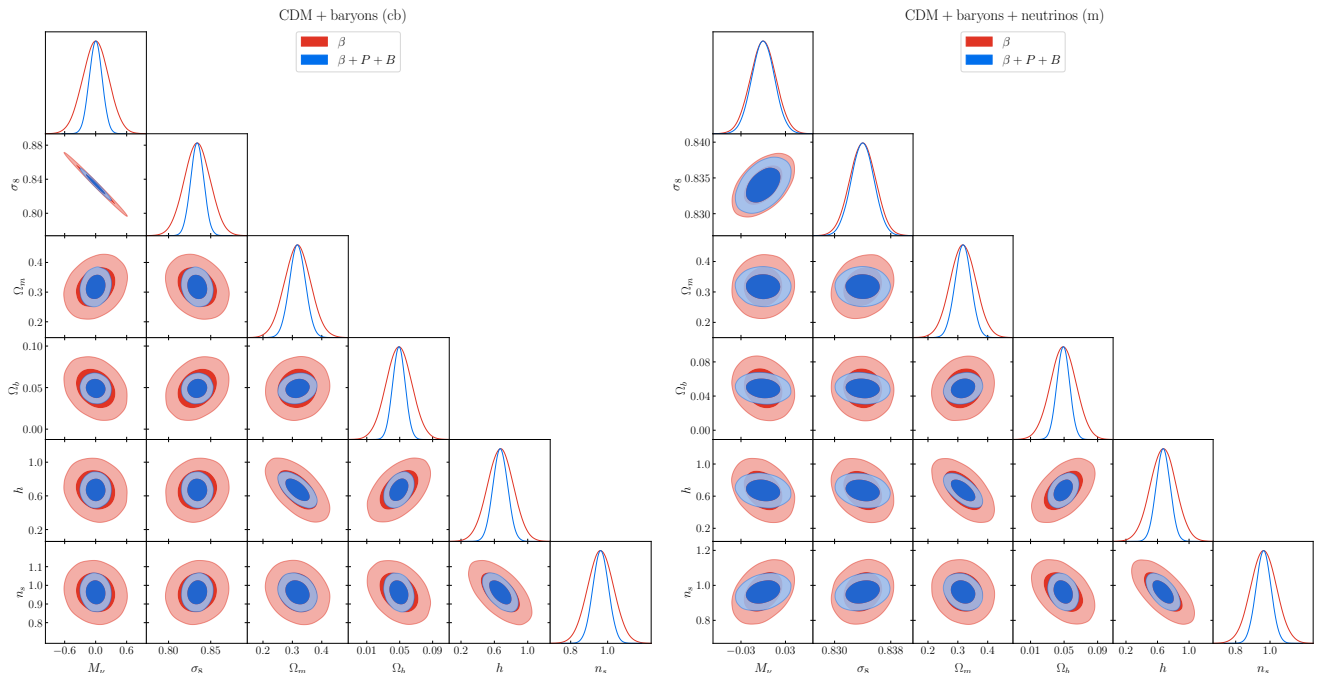


FIG. 8: Fisher forecasts for cosmological parameters. The left panel shows the confidence intervals on the cosmological parameters when the  $cb$  field is considered. The right panel is devoted to the total matter density field.

- J. R. P. Angel, L. Armus, D. Arnett, S. Asztalos, T. S. Axelrod, S. Bailey, *et al.*, arXiv preprint arXiv:0912.0201 (2009).
- [7] P. Ade *et al.* (Simons Observatory), JCAP **02**, 056 (2019), arXiv:1808.07445 .
- [8] K. N. Abazajian, P. Adshead, Z. Ahmed, S. W. Allen, D. Alonso, K. S. Arnold, C. Baccigalupi, J. G. Bartlett, N. Battaglia, B. A. Benson, *et al.*, arXiv preprint arXiv:1610.02743 (2016).
- [9] S. Dodelson, E. Gates, and A. Stebbins, *Astrophys. J.* **467**, 10 (1996), arXiv:astro-ph/9509147 .
- [10] S. Dodelson and M. Vesterinen, *Physical Review Letters* **103**, 171301 (2009), arXiv:0907.2887 .
- [11] J. Lesgourgues, G. Mangano, G. Miele, and S. Pastor, *Neutrino Cosmology* (2013).
- [12] K. N. Abazajian, *Phys. Rept.* **711-712**, 1 (2017), arXiv:1705.01837 [hep-ph] .
- [13] I. Esteban, M. C. Gonzalez-Garcia, M. Maltoni, T. Schwetz, and A. Zhou, *JHEP* **09**, 178 (2020), arXiv:2007.14792 [hep-ph] .
- [14] M. Aker *et al.* (KATRIN), *Nature Phys.* **18**, 160 (2022), arXiv:2105.08533 [hep-ex] .
- [15] J. Lesgourgues and S. Pastor, *Phys. Rept.* **429**, 307 (2006), arXiv:astro-ph/0603494 .
- [16] M. S. Madhavacheril, F. J. Qu, B. D. Sherwin, N. MacCrann, Y. Li, I. Abril-Cabezas, P. A. Ade, S. Aiola, T. Alford, M. Amiri, *et al.*, arXiv preprint arXiv:2304.05203 (2023).
- [17] Z. Pan, F. Bianchini, W. Wu, P. Ade, Z. Ahmed, E. Anderes, A. Anderson, B. Ansarinejad, M. Archipley, K. Aylor, *et al.*, arXiv preprint arXiv:2308.11608 (2023).
- [18] T. M. C. Abbott *et al.* (DES), *Phys. Rev. D* **107**, 083504 (2023), arXiv:2207.05766 .
- [19] T. Tröster *et al.* (KiDS), *Astron. Astrophys.* **649**, A88 (2021), arXiv:2010.16416 .
- [20] C.-T. Chiang, W. Hu, Y. Li, and M. Loverde, *Physical Review D* (2017).
- [21] C.-T. Chiang, M. Loverde, and F. Villaescusa-Navarro, *Physical review letters* **122** **4**, 041302 (2018).
- [22] T. Lazeyras, F. Villaescusa-Navarro, and M. Viel, *Journal of Cosmology and Astroparticle Physics* **2021**, 022 (2021), arXiv:2008.12265 .
- [23] E. Massara, F. Villaescusa-Navarro, S. Ho, N. Dalal, and D. N. Spergel, *Physical Review Letters* **126**, 011301 (2021), arXiv:2001.11024 .
- [24] W. Liu, A. Jiang, and W. Fang, *Journal of Cosmology and Astroparticle Physics* **2022**, 045 (2022), arXiv:2204.02945 .
- [25] W. Liu, A. Jiang, and W. Fang, *Journal of Cosmology and Astroparticle Physics* **2023**, 037 (2023), arXiv:2302.08162 .
- [26] C. D. Kreisch, A. Pisani, C. Carbone, J. Liu, A. J. Hawken, E. Massara, D. N. Spergel, and B. D. Wandelt, *Monthly Notices of the Royal Astronomical Society* (2018).
- [27] N. Schuster, N. Hamaus, A. Pisani, C. Carbone, C. D. Kreisch, G. Pollina, and J. Weller, *Journal of Cosmology and Astroparticle Physics* **2019**, 055 (2019).
- [28] S. Contarini, F. Marulli, L. Moscardini, A. Veropalumbo, C. Giocoli, and M. Baldi, arXiv: *Cosmology and Non-galactic Astrophysics* (2020).
- [29] P. Vielzeuf, M. Calabrese, C. Carbone, G. Fabbian, and C. Baccigalupi, *Journal of Cosmology and Astroparticle Physics* **2023** (2023).
- [30] C. Uhlemann, O. Friedrich, F. Villaescusa-Navarro, A. Banerjee, and S. Codis, *Monthly Notices of the RAS* **495**, 4006 (2020), arXiv:1911.11158 .
- [31] C. Hahn, F. Villaescusa-Navarro, E. Castorina, and

- R. Scoccimarro, *Journal of Cosmology and Astroparticle Physics* **2020**, 040 (2020), arXiv:1909.11107 .
- [32] G. A. Marques, J. Liu, J. M. Zorrilla Matilla, Z. Haiman, A. Bernui, and C. P. Novaes, *Journal of Cosmology and Astroparticle Physics* **2019**, 019 (2019), arXiv:1812.08206 .
- [33] J. Moon, G. Rossi, and H. Yu, *Astrophysical Journal* **264**, 26 (2023), arXiv:2302.03171 .
- [34] A. E. Bayer, F. Villaescusa-Navarro, E. Massara, J. Liu, D. N. Spergel, L. Verde, B. D. Wandelt, M. Viel, and S. Ho, *Astrophysical Journal* **919**, 24 (2021), arXiv:2102.05049 .
- [35] P. McMullen (1997).
- [36] S. Alesker, *Geometriae Dedicata* **74**, 241 (1999).
- [37] C. Beisbart, R. Dahlke, K. Mecke, and H. Wagner, in *Morphology of Condensed Matter*, Vol. 600, edited by K. Mecke and D. Stoyan (2002) pp. 238–260.
- [38] T. Matsubara, *The Astrophysical Journal* **584**, 1 (2003).
- [39] D. Hug, R. Schneider, and R. Schuster, *St Petersburg Mathematical Journal* **19**, 137 (2007).
- [40] T. Matsubara, C. Hikage, and S. Kuriki, *Physical Review D* **105**, 023527 (2022).
- [41] A. Cole and G. Shiu, *Journal of Cosmology and Astroparticle Physics* **2018**, 025 (2018), arXiv:1712.08159 .
- [42] G. Wilding, K. Nevenzeel, R. van de Weygaert, G. Vegter, P. Pranav, B. J. T. Jones, K. Efstathiou, and J. Feldbrugge, *Monthly Notices of the RAS* **507**, 2968 (2021), arXiv:2011.12851 .
- [43] S. Heydenreich, B. Brück, and J. Harnois-Déraps, *Astronomy and Astrophysics* **648**, A74 (2021), arXiv:2007.13724 .
- [44] S. Heydenreich, B. Brück, P. Burger, J. Harnois-Déraps, S. Unruh, T. Castro, K. Dolag, and N. Martinet, *Astronomy and Astrophysics* **667**, A125 (2022), arXiv:2204.11831 .
- [45] M. Tsizh, V. Tymchyshyn, and F. Vazza, *Monthly Notices of the RAS* **522**, 2697 (2023), arXiv:2301.09411 .
- [46] M. Biagetti, J. Calles, L. Castiblanco, A. Cole, and J. Noreña, *Journal of Cosmology and Astroparticle Physics* **2022**, 002 (2022), arXiv:2203.08262 .
- [47] T. K. Dey and Y. Wang, *Computational topology for data analysis* (Cambridge University Press, 2022).
- [48] H. Edelsbrunner and J. L. Harer, *Computational topology: an introduction* (American Mathematical Society, 2022).
- [49] A. J. Zomorodian, *Topology for computing* (Cambridge university press, 2005).
- [50] L. Wasserman, *Annual Review of Statistics and Its Application* **5**, 501 (2018).
- [51] N. Otter, M. A. Porter, U. Tillmann, P. Grindrod, and H. A. Harrington, *EPJ Data Science* **6**, 17 (2017).
- [52] C. M. Pereira and R. F. de Mello, *Expert Systems with Applications* **42**, 6026 (2015).
- [53] H. Masoomy, B. Askari, M. N. Najafi, and S. M. S. Movahed, *Physical Review E* **104**, 034116 (2021), arXiv:2101.03328 .
- [54] H. Masoomy, S. Tajik, and S. M. S. Movahed, *Physical Review E* **106**, 064115 (2022), arXiv:2208.12537 .
- [55] R. van de Weygaert, G. Vegter, H. Edelsbrunner, B. J. T. Jones, P. Pranav, C. Park, W. A. Hellwing, B. Eldering, N. Kruthof, E. G. P. P. Bos, J. Hidding, J. Feldbrugge, E. ten Have, M. van Engelen, M. Caroli, and M. Teillaud, in *Lecture Notes in Computer Science*, Vol. 6970 (2011) pp. 60–101.
- [56] X. Xu, J. Cisewski-Kehe, S. B. Green, and D. Nagai, *Astronomy and Computing* **27**, 34 (2019), arXiv:1811.08450 .
- [57] M. Biagetti, A. Cole, and G. Shiu, *Journal of Cosmology and Astroparticle Physics* **2021**, 061 (2021).
- [58] J. Cisewski-Kehe, B. T. Fasy, W. Hellwing, M. R. Lovell, P. Drozda, and M. Wu, *Physical Review D* **106**, 023521 (2022), arXiv:2204.00443 .
- [59] J. Feldbrugge, M. van Engelen, R. van de Weygaert, P. Pranav, and G. Vegter, *Journal of Cosmology and Astroparticle Physics* **2019**, 052 (2019), arXiv:1908.01619 .
- [60] O. H. E. Philcox and S. Torquato, *Physical Review X* **13**, 011038 (2023), arXiv:2207.00519 .
- [61] M. Nakahara, *Geometry, topology and physics* (CRC Press, 2003).
- [62] J. R. Munkres, *Elements of algebraic topology* (CRC Press, 2018).
- [63] F. Villaescusa-Navarro, C. Hahn, E. Massara, A. Banerjee, A. M. Delgado, D. K. Ramanah, T. Charnock, E. Giusarma, Y. Li, E. Allys, A. Brochard, C. Uhlemann, C.-T. Chiang, S. He, A. Pisani, A. Obuljen, Y. Feng, E. Castorina, G. Contardo, C. D. Kreisch, A. Nicola, J. Alsing, R. Scoccimarro, L. Verde, M. Viel, S. Ho, S. Mallat, B. Wandelt, and D. N. Spergel, *Astrophysical Journal* **250**, 2 (2020), arXiv:1909.05273 .
- [64] M. Zennaro, J. Bel, F. Villaescusa-Navarro, C. Carbone, E. Sefusatti, and L. Guzzo, *Monthly Notices of the RAS* **466**, 3244 (2017), arXiv:1605.05283 .
- [65] F. Villaescusa-Navarro, “Pylians: Python libraries for the analysis of numerical simulations,” *Astrophysics Source Code Library* (2018), ascl:1811.008 .
- [66] H. Hoekstra and B. Jain, *Annual Review of Nuclear and Particle Science* **58**, 99 (2008), arXiv:0805.0139 .
- [67] F. Marulli, C. Carbone, M. Viel, L. Moscardini, and A. Cimatti, *Monthly Notices of the RAS* **418**, 346 (2011), arXiv:1103.0278 .
- [68] E. Castorina, E. Sefusatti, R. K. Sheth, F. Villaescusa-Navarro, and M. Viel, *Journal of Cosmology and Astroparticle Physics* **2014**, 049 (2014), arXiv:1311.1212 .
- [69] S. Kaji, T. Sudo, and K. Ahara, arXiv e-prints , arXiv:2005.12692 (2020), arXiv:2005.12692 .
- [70] C. Maria, J.-D. Boissonnat, M. Glisse, and M. Yvinec, in *Mathematical Software–ICMS 2014: 4th International Congress, Seoul, South Korea, August 5-9, 2014. Proceedings 4* (Springer, 2014) pp. 167–174.
- [71] A. Lewis, arXiv e-prints , arXiv:1910.13970 (2019), arXiv:1910.13970 .
- [72] G. Papamakarios and I. Murray, arXiv e-prints , arXiv:1605.06376 (2016), arXiv:1605.06376 .
- [73] J. Alsing, T. Charnock, S. Feeney, and B. Wandelt, *Monthly Notices of the RAS* **488**, 4440 (2019), arXiv:1903.00007 .
- [74] K. Cranmer, J. Brehmer, and G. Louppe, *Proceedings of the National Academy of Science* **117**, 30055 (2020), arXiv:1911.01429 .